Biomechanics of the Human Posterior Sclera: Age- and Glaucoma-Related Changes Measured Using Inflation Testing

Baptiste Coudrillier,[1] *Jing Tian,*[2] *Stephen Alexander,*[1] *Kristin M. Myers,*[3] *Harry A. Quigley,*[4] *and Thao D. Nguyen*[1]

Purpose. The objective of this study was to measure the biomechanical response of the human posterior sclera in vitro and to estimate the effects of age and glaucoma.

Methods. Scleral specimens from 22 donors with no history of glaucoma and 11 donors with a history of glaucoma were excised 3 mm posterior to the equator and affixed to an inflation chamber. Optic nerve cross-sections were graded to determine the presence of axon loss. The time-dependent inflation response was measured in a series of pressure-controlled load–unload tests to 30 mm Hg and creep tests to 15 and 30 mm Hg. Circumferential and meridional strains were computed from the digital image correlation displacements, and midposterior stresses were determined from pressure and deformed geometry.

Results. Among normal specimens, older age was predictive of a stiffer response and a thinner sclera. In the age group 75 to 93, diagnosed glaucoma eyes with axon damage were thicker than normal eyes. Both damaged and undamaged glaucoma eyes had a different strain response in the peripapillary sclera characterized by a stiffer meridional response. Undamaged glaucoma eyes had slower circumferential creep rates in the peripapillary sclera than normal eyes. Glaucoma eyes were not different from normal eyes in stresses and strains in the midposterior sclera.

Conclusions. The observed differences in the biomechanical response of normal and glaucoma sclera may represent baseline properties that contribute to axon damage, or may be characteristics that result from glaucomatous disease. (*Invest Ophthalmol Vis Sci.* 2012;53:1714–1728) DOI:10.1167/iovs.11-8009

From the [1]Department of Mechanical Engineering, the [2]Biostatistics Consulting Center, School of Public Health, and the [4]Glaucoma Center of Excellence, Wilmer Ophthalmological Institute, School of Medicine, The Johns Hopkins University, Baltimore, Maryland; and the [3]Department of Mechanical Engineering, Columbia University, New York, New York.

Supported in part by Public Health Service Research Grants EY021500 (TDN), EY02120 and EY01765 (HAQ and Wilmer Institute), the Leonard Wagner Charitable Trust, William T. Forrester, and Saranne and Livingston Kosberg.

Submitted for publication June 7, 2011; revised October 14 and November 30, 2011, and January 26, 2012; accepted January 31, 2012.

Disclosure: **B. Coudrillier**, None; **J. Tian**, None; **S. Alexander**, None; **K.M. Myers**, None; **H.A. Quigley**, None; **T.D. Nguyen**, None

Corresponding author: Thao D. Nguyen, Department of Mechanical Engineering, The Johns Hopkins University, Baltimore, MD 21218; vicky.nguyen@jhu.edu.

Glaucoma damage is characterized by the loss of retinal ganglion cells (RGC) leading to permanent vision loss. The level of intraocular pressure (IOP) strongly correlates with the incidence and prevalence of open angle glaucoma (OAG) and the severity of glaucomatous damage to the optic nerve head (ONH).[1–3]. The biomechanical response of the ONH to IOP is determined by the geometry and mechanical properties of the sclera and lamina cribrosa (LC).[4–6] Finite element modeling studies of the posterior sclera have suggested that the elastic modulus of the sclera significantly influences the level of strains developed in the LC.[7] Several factors mediate the scleral response to IOP. For example, aging and disease may influence scleral connective tissue properties, thereby altering the stress and strain environment of the ONH. The effects of glaucoma may produce alterations to the scleral material properties over time, either mitigating or contributing to RGC damage. The tissues of the sclera and LC stiffen with age in monkey,[8] mouse,[9] and human[10] eyes. In human glaucomatous tissue, alterations occur in the extracellular matrix (ECM) structure of the LC. Transmission electron microscopy of the LC showed alterations to the density and distribution of the collagen structure[2] and to the morphology of the elastin fibers. The latter become dissociated from other connective tissue elements with increasing glaucoma damage.[11]

In addition to these anatomic findings, mechanical testing has revealed that the sclera of glaucoma eyes differs from normal eyes. Using uniaxial strip tests, Downs et al.[12] measured a larger relaxation time and higher equilibrium modulus for monkey eyes with early glaucoma. Hommer et al.[13] reported an increase in a parameter estimating ocular rigidity in vivo in OAG eyes. Girard et al.[14] found that scleral tangent modulus decreased with small chronic IOP elevation and increased with large chronic IOP elevations in monkey eyes in vitro. Axial elongation of the eye has been observed in experimental mouse glaucoma.[15] The difference in axial elongation among types of mice subjected to experimental glaucoma leads to the possibility that there are definable interactions between baseline scleral properties and the effects of chronic IOP elevation on the ocular connective tissues. Increased creep response has also been measured for the sclera of elongated eyes from induced myopia in chickens.[16] The increased risk for OAG from myopia may relate in part to scleral mechanical properties.[17]

Past modeling studies have treated the scleral tissue as an elastic[6,7] or a hyperelastic[14,18] material, ignoring potential rate dependence and creep behavior. However, the time-dependent properties of the sclera and ONH may be important because they dictate the biomechanical response of the ONH to short-term pressure fluctuations. Previous research with in vivo characterization of the time-dependent mechanical response of the eye includes ocular creep tests on animal models.[16] In vivo methods provide the structural response of the entire eye,

Table 1. Age Distribution and Nerve Grade for Donors of Normal and Diagnosed Glaucoma Eyes

	No History of Glaucoma			Diagnosed Glaucoma				
Damage	Normal	Mild	Unknown	Normal	Mild	Intermediate	Severe	Unknown
Axon Loss	<10%	0%–25%	—	<10%	10%–25%	25%–50%	50%–75%	—
Age 40–49	2/1*	—	4/2	—	—	—	—	—
Age 50–59	4/3	—	—	—	—	—	—	—
Age 60–69	1/1	2/1	3/2	3/2	—	—	—	1/1
Age 70–79	11/7	—	4/4	2/2	—	1/1	—	2/2
Age 80–93	1/1	—	3/2	6/4	3/3	—	3/2	1/1
Total	19/13	2/1	14/10	11/8	3/3	1/1	3/2	4/4

* 2/1 indicates that two eyes from one donor were tested. Thirty-five normal eyes from 22 donors and 22 diagnosed glaucoma eyes from 11 donors were included in this study. Note that the number of donors cannot be summed as some donors had different grades for the right and left eye and were listed twice.

whereas in vitro methods allow the mechanical response of the sclera to be evaluated separately from other ocular components. For some highly cellular tissues, in vitro tests have been associated with postmortem tissue degradation. However, a previous study by Girard[19] using uniaxial tensile tests showed little difference in the viscoelastic material properties measured for fresh scleral tissue and tissue stored in saline solution at 4°C and tested within 72 h of enucleation. Previous in vitro uniaxial tensile tests of strip specimens of monkey,[12] rabbit,[19] and tree shrew[16] sclera provided direct measurements of the stress-strain behavior and material properties; however, they did not reproduce the complex physiological loading conditions of the eye in its three-dimensional configuration. Furthermore, the cutting of curved tissue into flat strips and the clamping of the tissue into tensile testing jaws disrupted the native fiber structure and the natural curvature of the tissue. In vitro inflation testing of intact scleral tissue was developed as an improvement to the uniaxial strip test methodology.[20]

In the present study, we measured the inflation response of isolated posterior sclera of normal and glaucomatous human eyes subjected to time-dependent and rate-dependent inflation tests and developed an analytical method for strain and midposterior stress calculations. Differences in the biomechanical response between the sclera of glaucoma eyes and those of normal eyes provided macroscopic evidence of natural and/or glaucoma-induced alterations of the ECM associated with both aging and glaucoma.

Methods

Eye Tissues

Thirty-five pairs of donor eyes were obtained from the National Disease Research Interchange (NDRI) from 11 persons with a clinical diagnosis of glaucoma and from 24 persons whose hospital records showed no history of glaucoma. Eyes designated here as diagnosed glaucoma were donated postmortem in persons whose medical records showed a coded diagnosis of glaucoma, who were prescribed known IOP lowering medications in hospital records, and/or whose family confirmed that the deceased had been treated for glaucoma. Controls had no history of any of these factors. There were slightly more female than male donors (19 female donors). The mean age of normal donors (67.5 ± 13.3) was younger than that of glaucoma donors (80.5 ± 9.3); however, we obtained and tested a similar number of normal eyes in the age range of the glaucoma donors (Table 1, *2/1 indicates that two eyes from one donor were tested). We confirm that our research followed the tenets of the Declaration of Helsinki.

The eyes were received packed in ice, preserved in balanced salt solution (BSS, Alcon, Inc., Fort Worth, TX) and tested within 72 hours of death.[19] From the 35 pairs of donated eyes, only specimens from age 40 and older were used in this study (33 pairs). Fifty-seven scleral specimens were ultimately inflation tested, and nine were discarded because leakage was detected during testing. Optic nerve cross-sections were taken 1–3 mm behind the eye from each specimen prior to testing and fixed in a 4% paraformaldehyde solution (Electron Microscopy Sciences, Hatfield, PA) prior to embedding in epoxy resin and sectioning at 1 μm thickness. A glaucoma specialist (HQ), experienced in optic nerve grading and masked to the diagnosis, assigned a quantitative grade from 0 to 4 for the degree of axon loss[21] (Table 1). The assigned grades 0 to 4 corresponded to 10% or less loss (normal appearance), 10% to 25% loss (mild damage), 25% to 50% loss (intermediate damage), 50% to 75% loss (severe damage), and 75% or more loss (total damage). There were no grade 4 nerves present in this study. Some nerves had preservation that was too poor for grading and were labeled as ungradable.

Sample Preparation

The surrounding fat, muscle, and episcleral tissues were gently removed. The optic nerve was excised with a razor blade flush with the sclera and preserved in paraformaldehyde as described above. The eye was kept moist with BSS during preparation. The axial length, nasal–temporal diameter, and superior–inferior diameters of the intact eye were measured with a digital caliper (Fig. 1). Each measurement was made three times (SD: 0.3 mm). The sclera was firmly glued to a custom plastic ring 3 mm posterior to the equator using cyanoacrylate, carefully positioned in the fixture to center the ONH (Fig. 1). Three different ring sizes were available to fit the diameters of different eyes. The anterior sclera, cornea, and lens were excised and removed. To promote a water-tight seal and prevent leakage during testing, the scleral rim was scored and impregnated with cyanoacrylate. Examination after testing showed that the glue did not diffuse into the sclera. After the glue dried, the vitreous, retina, and choroid were removed from the posterior scleral specimen. Figure 2b shows an example of the posterior sclera mounted on the fixture.

Experimental Setup and Loading Regimen

The inflation response of scleral samples was measured by adapting a method developed previously for bovine cornea[22] and sclera.[23] In brief, the sclera and fixture were mounted on a pressure chamber and inflated via pressure-controlled injection of BSS. The pressure in the chamber was monitored using a pressure transducer (Honeywell, Sensing and Control, Morristown, NJ, precision: 0.15 mm Hg) and adjusted through active feedback control of an automated injection system (TestWorks 4, MTS Insight, Eden Prairie, MN). As shown in Figure 2b, the thickness was measured at eight locations in the peripapillary sclera 2 mm from the ONH and at eight locations in the midposterior sclera at middistance between the ONH and the holder using an ultrasonic pachymeter designed for corneal thickness

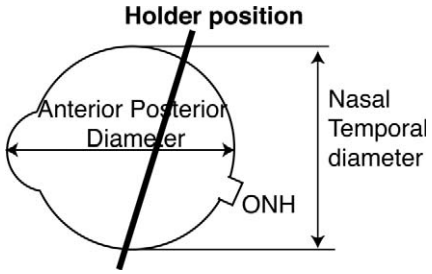

Figure 1. The position of the holder (thick line) glued to the scleral specimen and the standard position of the ONH during testing.

measurements (DGH Technology, Inc., Exton, PA). To account for the difference in the speed of sound of the sclera $c_s = 1622$ m/s[24] and the cornea $c_c = 1640$ m/s (default value of the pachymeter), the measurements were multiplied by a correction factor $r = c_s/c_c$. The reported thickness at each location was the average of 50 measurements performed at 15 mm Hg. The standard deviation of the 50 measurements was less than 15 μm. The scleral surface was speckled by dispersing graphite powder through a 62-μm mesh to provide a high contrast pattern for digital image correlation (DIC). A previous study on bovine sclera showed that the graphite powder did not degrade the tissues during the time of testing.[23] Dispersing the graphite particles through a mesh allowed for better control of the particle density, which reduced the correlation error. Figure 2c shows an image of the speckled sclera mounted on the inflation chamber. A humidity chamber was fitted on top of the pressure chamber to mitigate the effects of tissue dehydration during testing. This ensured that the pressure–displacement response was unchanged over time. The humidity chamber was closed with a thin transparent glass cover and filled with water-logged insulation material. The specimens were tested at room temperature (24 ± 1°C).

Each specimen was subjected first to three load–unload cycles from the reference pressure of 1.5 to 30 mm Hg at a pressure rate of 1 mm Hg/s. Preliminary results showed buckling of some scleral specimens below 1.5 mm Hg near the holder. In addition, measuring the response of the sclera at low pressures increased the accuracy of the model fit presented below. The pressure was held constant at the reference pressure for 15 minutes between each cycle to allow for full recovery of the displacements. The rate-dependence of the tissue was evaluated by performing another load–unload cycle at a pressure rate of 0.05 mm Hg/s. Finally, the specimen was subjected to two ramp-hold creep tests at 15 and 30 mm Hg. In each test, the loading rate was 1 mm Hg/s. The pressure was held for 20 minutes, and the specimen was allowed to recover for 30 minutes at the reference pressure after unloading. Full recovery was achieved after each test.

Digital Image Correlation

During testing, the deforming scleral surface was imaged by two charge-coupled device cameras at a rate of 0.5 frames per second (Pt. Grey Research GRAS-20SM/C, Schneider Kreuznach 35 mm lens, f8; VicSnap, Correlated Solutions, Inc., Columbia, SC). The cameras were positioned 50 cm above the specimen and oriented 15° from the vertical axis on opposite sides. The scleral surface was transilluminated with four fiber optic lights entering the bottom of the chamber. The light source was diffused by a silicon oil diffuser lining the bottom of the pressure chamber. The images were analyzed by a commercial DIC program (Vic3D, Correlated Solutions, Inc., Columbia, SC) to calculate the 3D displacement map of the scleral surface. The reference (undeformed) configuration was defined by the image taken at the reference pressure of 1.5 mm Hg. The displacements were calculated by correlating the gray value of a subset of pixels of each deformed image to subsets of pixels of the reference image. On average, speckling patterns covered at least 100 gray levels out of the 256 available. The position of the material points of the scleral surface were reported in terms of the *X, Y,* and *Z* Cartesian coordinates, and the displacements of these points were reported in terms of the Cartesian

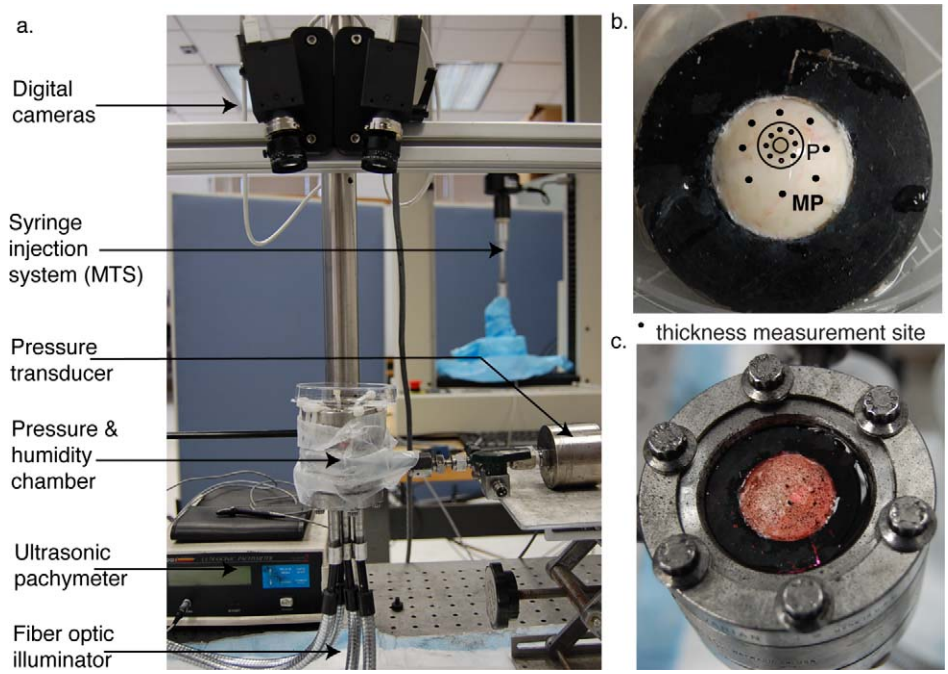

Figure 2. (**a**) Experimental setup. Two charge-coupled device cameras imaged the posterior sclera, which was inflated by pressure-controlled injection of BSS. (**b**) Posterior sclera glued on the holder 3 mm posterior to the equator. Black dots indicate the location of thickness measurements. These were grouped into two circles of radius 2 and 10 mm centered at the ONH, representing the peripapillary and midposterior region, starting from the nasal pole. The ONH does not appear centered because of the camera angle. (**c**) The specimen transilluminated and speckled with graphite powder for digital imaging correlation.

Table 2. Uncertainty in the DIC Out-of-Plane Displacement Measurements

Stage Displacement	Entire Sclera		Central Sclera		Peripheral Sclera	
	Avg DIC Displacement (μm)	SD (μm)	Avg DIC Displacement (μm)	SD (μm)	Avg DIC Displacement (μm)	SD (μm)
1.0008 μm	2.2	2.0	2.1	1.3	2.8	2.4
1.988 μm	3.4	2.0	2.7	1.5	3.5	2.8
5.012 μm	4.6	2.0	4.5	1.8	5.5	3.0
9.996 μm	10.3	2.0	10.2	1.9	10.5	3.5
19.992 μm	19.0	2.0	18.9	2.4	20.4	7.0
50.008 μm	49.5	3.0	50.4	3.1	50.1	12.3
200.012 μm	197.1	4.0	197.3	3.2	200.1	6.2

components u_x, u_y, and u_z of the displacement vector. With a 15° stereo-angle and a focal length of 35 mm, the predicted variability in out-of-plane position measurements was 20 μm.[25]

To evaluate the intrinsic uncertainty of the DIC system in out-of-plane displacement measurements, a speckled piece of sclera was glued on a ping-pong ball. The specimen was placed on the stage of a micromanipulator that could be translated vertically by steps of 28 nm. The stage was moved from the reference position to a final vertical position of 1.008, 1.988, 5.012, 9.996, 19.992, 50.008, and 200.012 μm in repeats of five. Table 2 compares the norm of the DIC measured displacement and the applied displacement of the stage for three regions: (1) over the entire sclera, (2) over the central region defined as the circle of 1 mm in diameter centered on the apex, and (3) over the peripheral region defined as the annulus of 0.5 mm of the sclera closest to the equator of the ping-pong ball. The out-of-plane displacements were calculated with a maximum uncertainty of 8 μm (95% confidence interval) over the entire sclera; however, the resolution decreased in the peripheral sclera, probably due to curvature effects and poorer lighting conditions. Because we used the same speckling techniques and similar lighting conditions in this experiment and in the inflation tests, we estimated the uncertainty in the displacement calculation to be not greater than 8 μm.

Strain and Stress Analysis

The magnitude of the measured displacements depends on the dimensions of the scleral cup and the dimensions and locations of the ONH and holder in the scleral cup. For example, positioning the holder more anterior toward the equator would increase the displacements measured near the ONH. Because of these geometry and boundary effects, the pressure–displacement response cannot be used to compare the mechanical properties of the sclera of different specimens to evaluate the effects of age or glaucoma. The constitutive behavior of a material, which relates states of stress and strain, is determined solely by the mechanical properties of the material and is independent on the geometry and loading conditions. Strains are a normalized measure of deformation. The normal strain describes the elongation of a material line relative to the original length, while the shear strain describes the change in angle between two material lines. For a thin membrane, the normal stresses describe how the pressure-induced tensile forces are distributed in the scleral wall. In the following, we present analytical models to calculate strains from the DIC displacements and stresses from the deformed specimen dimensions and applied pressure. We then present a constitutive model for the nonlinear, anisotropic stress–strain behavior of the tissue and define different stiffness measurements for statistical comparisons.

Developing constitutive relations for scleral and corneal tissues from inflation measurements has been a main focus of recent research in ocular biomechanics. Anderson et al.[26] developed an analytical method based on shell theory to study the mechanical response of the cornea during inflation. This model assumed a spherical geometry, constant thickness, and homogeneous material behavior, and included the contribution of the corneal bending stiffness. A more detailed approach used inverse finite element analysis, which additionally can consider regional variations in the material properties, thickness, and curvature, to derive the material properties of bovine cornea[34] and the aging monkey eye[8] from inflation tests. While this may provide a more accurate description of scleral mechanics, comparing the obtained map of parameters for age and disease effects would likely produce statistical analysis results that are difficult to interpret. In addition, the associated computational costs make the method intractable for large-scale studies (57 eyes). We chose an analytical method to determine the stress–strain relationship and material properties of our scleral specimens. The method improves upon the early mathematical models in two ways. It does not assume a spherical topography or constant thickness, and it accounts for the experimentally observed anisotropic and nonlinear behavior. The strains were locally calculated from the DIC displacement gradients. The stresses in the midposterior sclera were calculated from the pressure and local thickness and curvature. For the purpose of statistical analysis, strains and stresses were averaged over the entire midposterior region to obtain a representative stress–strain curve that was fitted to a constitutive model. Similarly, for each specimen, the peripapillary scleral strains were averaged to obtain a mechanical outcome. The material parameters and the averaged strains in the peripapillary sclera provided convenient biomechanical measures for statistical comparison. While this method could be used to determine regional variations of material parameters, these were not accounted for in the statistical analysis.

Strains in the Midposterior Sclera. Figures 3a and 3b show a diagram of the scleral specimen and the location of the midposterior region. We fit a sphere to the midposterior region of the undeformed specimen and introduced a spherical coordinate system ($\mathbf{e}_R$, $\mathbf{e}_\varphi$, $\mathbf{e}_\theta$), where φ is the meridional direction connecting the ONH to the holder, θ is the circumferential direction, and R is the radius of the spherical fit. The experiments measured the Cartesian components u_x, u_y, u_z of the displacement vector $\mathbf{u}$ for a rectangular grid. To calculate the strains in the circumferential and meridional directions, we created a spherical grid with points every 0.5° in the circumferential and meridional directions for the undeformed specimen and extrapolated u_x, u_y, and u_z to the spherical grid. The Cartesian components were transformed to the spherical coordinate system and smoothed using an open source MatLab function *gridfit* (MatLab R2010b, MathWorks, Natick, MA, by J. D'Errico) to obtain the radial u_R, meridional u_φ, and circumferential u_θ displacements at the grid points. We also defined tangent vectors $\mathbf{T}_\theta = \mathbf{e}_\theta$ and $\mathbf{T}_\varphi = \mathbf{e}_\varphi$ to the undeformed circumference and meridian at each grid point. The tangent vectors to the deformed circumference and meridian were calculated from the displacement vector as,

$$\mathbf{t}_\theta = \mathbf{T}_\theta + \frac{1}{R\sin\varphi}\frac{\partial \mathbf{u}(X)}{\partial \theta}, \quad \mathbf{t}_\varphi = \mathbf{T}_\varphi + \frac{1}{R}\frac{\partial \mathbf{u}(X)}{\partial \varphi}. \qquad (1)$$

The displacement gradients were computed for the spherical grid using central difference. The stretch in the circumferential and meridional directions were computed from the magnitude of the

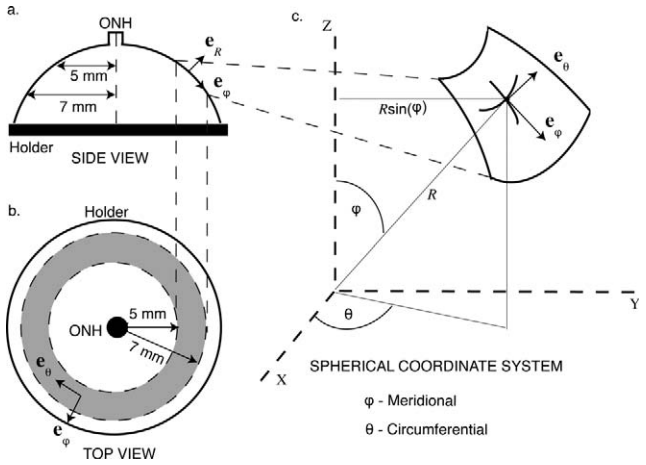

Figure 3. (**a**) Side view of the posterior sclera with representation of the midposterior region. (**b**) Camera view. (**c**) Definition of the spherical coordinate system to describe the position of points of the midposterior scleral surface. The circumferential direction $\mathbf{e}_\theta$ is parallel to the holder and the meridional direction $\mathbf{e}_\varphi$ is tangent to the meridian and perpendicular to $\mathbf{e}_\theta$.

deformed tangent vectors, $\lambda_\theta = ||\mathbf{t}_\theta||$ and $\lambda_\varphi = ||\mathbf{t}_\varphi||$, and the Green-Lagrange strains were calculated from the stretches as,

$$E_{\theta\theta} = \frac{1}{2}(\lambda_\theta^2 - 1), \quad E_{\varphi\varphi} = \frac{1}{2}(\lambda_\varphi^2 - 1). \tag{2}$$

For small strains, equation 2 reduces to the familiar relations $E_{\theta\theta} = (\lambda_\theta - 1)$ and $E_{\varphi\varphi} = (\lambda_\varphi - 1)$. The circumferential strain $E_{\theta\theta}$ and meridional strain $E_{\varphi\varphi}$ describe the point-wise elongation of the circumference and the meridian during the inflation test. The shear strain, defined as $E_{\theta\varphi} = \frac{1}{2}\mathbf{t}_\theta \cdot \mathbf{t}_\varphi$, describes the relative distortion of the initially orthogonal meridional and circumferential directions. In the midposterior sclera, the ratio of the regionally averaged shear strains to the averaged normal strains was 0.067 ± 0.052 (less than 10%, Appendix B). The relatively small in-plane shear strains were neglected in the remainder of the analysis. Away from the holder and the ONH, the other shear strain components $E_{\theta r}$ and $E_{\varphi r}$ were assumed to be negligible, though this assumption could not be verified because the DIC method measured only the surface displacements.

Strains in the Peripapillary Sclera. The surface of the peripapillary region had a nonspherical geometry caused by the transition of the sclera to the optic nerve sheath and the presence of the dura and other remnant tissues. In the smoothed method presented above for the midposterior sclera, the z-position of the surface grid points was obtained from the spherical fit. In the peripapillary sclera, we defined a similar circumferential and meridional grid, where the z-position was calculated directly from the DIC data. Cartesian displacements were interpolated to the points of the grid and smoothed using the same MatLab function described previously. As shown in Figures 4b and 4c, we defined L_θ as the length measured between two adjacent grid points in the circumferential direction marked on the undeformed grid and l_θ as the length between the same points on the deformed peripapillary sclera. Similarly, L_φ and l_φ were the lengths measured between two adjacent grid points in the meridional direction on the undeformed and deformed peripapillary sclera. The stretches in the circumferential and meridional directions were defined as the ratio of the deformed length over the undeformed length, $\lambda_\theta = l_\theta/L_\theta$ and $\lambda_\varphi = l_\varphi/L_\varphi$. The strains were calculated from the stretches using equation 2. This method was identical to the smoothed method in the limit of an infinitely dense grid. We compared the two methods in the midposterior sclera for a grid marked every 0.5° in the meridional and circumferential directions and obtained negligible differences. Shear deformations that likely developed in the peripapillary sclera were not addressed in this study.

Meridional and Circumferential Stresses in the Midposterior Sclera. During inflation, it was possible that the shape of the midposterior sclera did not remain spherical. To determine the circumferential and meridional stresses $\sigma_{\theta\theta}$ and $\sigma_{\varphi\varphi}$, we modeled the deformed midposterior sclera as a thin ellipsoidal membrane of revolution (Fig. 5). The thin assumption neglects the stress components normal to the surface of the shell and also the through-thickness variations of the membrane stress components. We also assumed that the effect of shear and bending were negligible in the midposterior region. As a result, the stress components of a thin, axisymmetric membrane subjected to an internal pressure p can be determined solely from equilibrium.[27]

$$\boldsymbol{\sigma}_{\varphi\varphi} = \frac{pr_2}{2t}, \quad \boldsymbol{\sigma}_{\theta\theta} = pr_2\frac{2r_1 - r_2}{2r_1 t}, \tag{3}$$

where t is the deformed thickness, r_1 is the radius of curvature of the deformed meridian, and r_2 is the transversal curvature. For an ellipsoid of revolution, the radii of curvature can be determined from the semimajor axis a and the semiminor axis b as,[27]

$$r_1 = \frac{a^2b^2}{(a^2\sin^2\varphi + b^2\cos^2\varphi)^{3/2}}, \qquad r_2 = \frac{a^2}{(a^2\sin^2\varphi + b^2\cos^2\varphi)^{1/2}}. \tag{4}$$

To calculate the circumferential and meridional stress components at each point, an ellipsoid of revolution was fitted to the deformed coordinates of the midposterior sclera at each pressure step to obtain the semimajor axis a, and the semiminor axis b (*Ellipsoid_fit* by Yury Petrov, MATLAB Central File Exchange, May 2011). These were used to calculate the local radii of curvature according to equation 4. To calculate the deformed thickness t_p at the pressure step p, we used the measured thickness at 15 mm Hg t_{15} and the assumption of incompressibility,

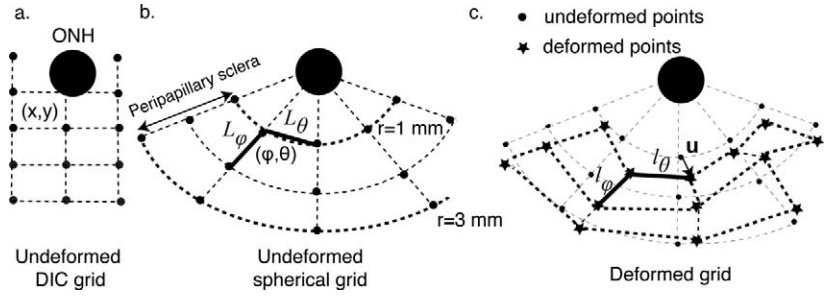

Figure 4. (**a**) 2D projection of the DIC grid of points of the undeformed surface. (**b**) 2D projection of the new grid with points aligned in the circumferential and meridional directions. The distance between two consecutive points in $\mathbf{e}_\varphi$ is L_φ. (**c**) 2D projection of the deformed grid. The new distance between the same points in the deformed configuration is l_φ. The meridional stretch was calculated as $\lambda_\varphi = l_\varphi/L_\varphi$.

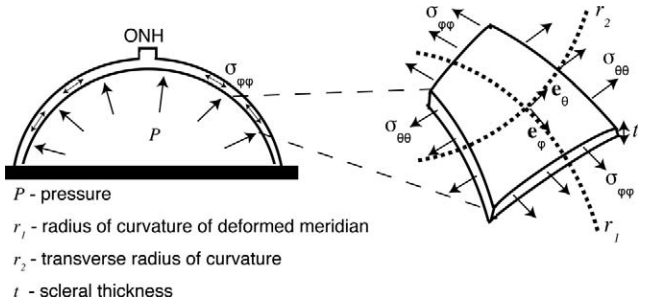

Figure 5. Membrane stresses are generated in the sclera to equilibrate the applied pressure. They can be calculated from the pressure, thickness of the sclera, and two principal radii of curvature.

$$t_p = t_{15}\frac{\lambda_\theta(15)\lambda_\varphi(15)}{\lambda_\theta(p)\lambda_\varphi(p)}. \tag{5}$$

The experimental thickness was measured at eight locations in the midposterior sclera. Points of the same sector were attributed the same thickness value. In the peripapillary sclera, the stresses cannot be determined using the thin membrane model because of the presence of the compliant ONH. Consequently, we only present the pressure-strain response for the peripapillary region.

Anisotropic Hyperelastic Constitutive Model for the Midposterior Sclera. The midposterior sclera was modeled as a composite material with fibrillar components aligned with the meridional direction $\mathbf{e}_\varphi$ and the circumferential direction $\mathbf{e}_\theta$ embedded in an isotropic incompressible matrix of proteoglycans.[37] The nonlinear stress–stretch relation of the model is given by:

$$\begin{aligned}\boldsymbol{\sigma}_{\theta\theta} &= \mu\left(\lambda_\theta^2 - \frac{1}{\lambda_\theta^2\lambda_\varphi^2}\right) + 2\alpha_\theta\lambda_\theta^2\left[\exp\left(\beta(\lambda_\theta^2-1)\right)-1\right],\\ \boldsymbol{\sigma}_{\varphi\varphi} &= \mu\left(\lambda_\varphi^2 - \frac{1}{\lambda_\theta^2\lambda_\varphi^2}\right) + 2\alpha_\varphi\lambda_\varphi^2\left[\exp\left(\beta(\lambda_\varphi^2-1)\right)-1\right].\end{aligned} \tag{6}$$

The derivation of this constitutive relation is detailed in Appendix A.A set of four parameters described the nonlinear, anisotropic mechanical response of the sclera:

(1) μ is the shear modulus of the matrix, which was set to 20 kPa[28] to limit the number of parameters for the fitting procedure,

(2) $M_\theta = 4\alpha_\theta\beta$ denotes the stiffness of the circumferential fiber family,

(3) $M_\varphi = 4\alpha_\varphi\beta$ denotes the stiffness of the meridional fiber family, and

(4) β is a stiffening parameter that characterizes the nonlinearity of the stress–stretch response. A higher β causes the stress–strain relation to stiffen at smaller strains. The same value of β was used for both fiber families.

The ratio of the fiber stiffnesses M_θ and M_φ was used to evaluate the degree of anisotropy of the tissue. The stresses and strains calculated for the first loading cycle were averaged over the entire midposterior region. Equation 6 was fitted to the averaged stress–stretch curve to evaluate the material parameters. The fitting procedure was formulated as the minimization of the objective function C:

$$C(\alpha_\theta,\alpha_\varphi,\beta) = \sum_{p=1}^{n_{\text{steps}}}\left[\left(\boldsymbol{\sigma}_{\varphi\varphi}^{\text{exp}} - \boldsymbol{\sigma}_{\varphi\varphi}^{\text{model}}(\lambda_\theta^{\text{exp}},\lambda_\varphi^{\text{exp}},\alpha_\theta,\alpha_\varphi,\beta)\right)_p^2 + \left(\boldsymbol{\sigma}_{\theta\theta}^{\text{exp}} - \boldsymbol{\sigma}_{\theta\theta}^{\text{model}}(\lambda_\theta^{\text{exp}},\lambda_\varphi^{\text{exp}},\alpha_\theta,\alpha_\varphi,\beta)\right)_p^2\right]. \tag{7}$$

where $n_{\text{steps}} = 15$ is the number of pressure steps during the loading curve. The values of α_θ, α_φ, and β were calculated using a quasi-Newton method from an optimization MatLab function (*sqp algorithm*, *fmincon*, MatLab R2010b). Figure 6 illustrates the ability of the model to fit the experimental data for one specimen of age 77. A single set of parameters was calculated for each eye to provide a convenient measure of the material response of the sclera for statistical comparison.

Biomechanical Measures

For each of the 57 specimens, the circumferential strain $E_{\theta\theta}$ and meridional strain $E_{\varphi\varphi}$ were calculated at 22.5 mm Hg in the peripapillary and midposterior regions. The average strains for each region were used as indicators of the structural stiffness of the sclera. In addition, the circumferential and meridional stresses and stretches were calculated in the midposterior sclera at every pressure step of the first loading cycle and averaged over the entire region. The constitutive model (equation 6) was fitted to the averaged stress–stretch data to determine the fiber stiffnesses M_θ and M_φ and the stiffening parameter β for each specimen. In the midposterior sclera, we defined the anisotropy as the ratio M_θ/M_φ. The anisotropy describes the effect that the relative amount of fibers oriented in the circumferential and meridional directions had on the overall mechanical behavior of the tissue. In the peripapillary sclera, the ratio of the meridional to circumferential strain was used to compare the combined effects of the geometry and anisotropic material properties of the sclera and ONH to the mechanical response. For the creep tests to 15 and 30 mm Hg, the circumferential and meridional strains were calculated at time 20, 40, 60, 80, 160, 460, 560, 760, 960, 1160 seconds in the peripapillary and midposterior sclera. In each region, the strain creep rates were defined as the slope of the average strain versus time curve plotted on a log–log scale.

Statistical Analysis

Multivariate regression models were constructed using data from all normal specimens to estimate the effects of age on the average

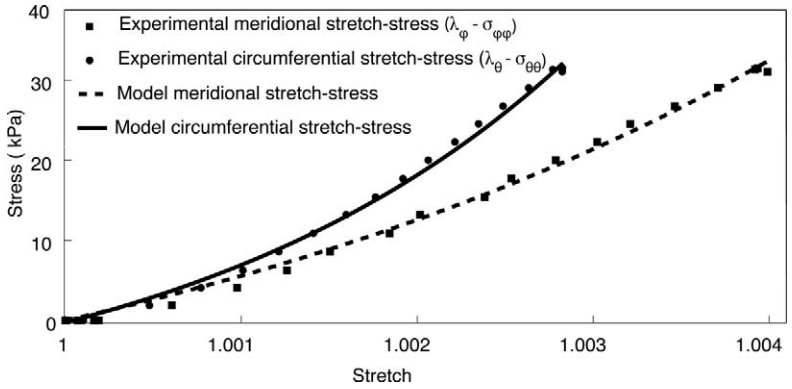

Figure 6. Stress–stretch response averaged over the midposterior sclera for a normal sclera (age 77). Comparison of experimental results (dots) and model fit (lines).

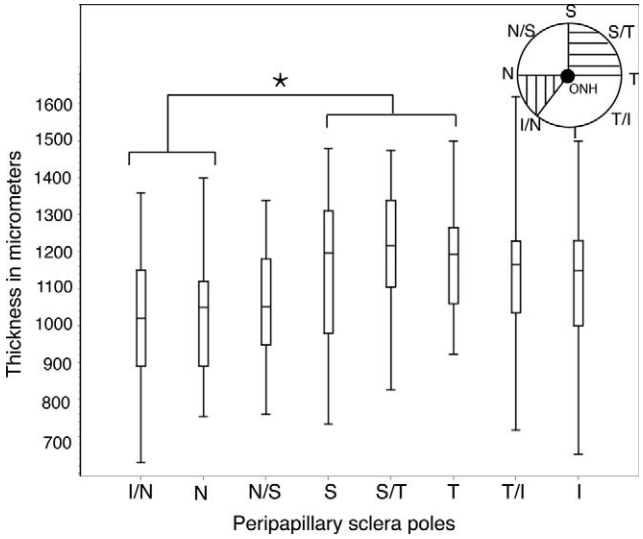

Figure 7. Box plots of the local average thickness in the peripapillary sclera for normal specimens. N, indicates nasal; S, superior; T, temporal; I, inferior; and N/S, means that the location site was in between nasal and superior. Thickness measurements were performed 2 mm from the center of the nerve head. The I/N and N poles were significantly thinner (* indicates $P \leq 0.005$) than the S, S/T, and T poles as shown in the schematic on the top right.

outcomes. Region of the sclera, midposterior or peripapillary sclera when applicable, and age were used as predictors. For the comparison between normal and glaucoma specimens, glaucoma eyes were divided into two categories. Diagnosed glaucoma eyes whose optic nerves were graded as having ≤10% axon loss were labeled as undamaged (11 eyes from 8 donors, average age ± SD: 79.8 ± 10.4). Glaucoma eyes with optic nerve gradings of mild, moderate, or severe damage formed the second category, labeled as damaged glaucoma (7 eyes from 5 donors, average age ± SD: 83.1 ± 4.1). Normal eyes were included, whether their nerves were gradable or not (35 eyes from 22 donors, average age ± SD: 69.0 ± 13.5). In order to account for the age distribution of the normal and glaucoma eyes, comparisons of the outcomes were performed within two age groups: 60 to 75 years and 76 to 93 years. Repeated measures ANOVA was used to compare the outcomes of the three groups. In a final model, age and diagnoses of glaucoma were added together as variables in a multivariate regression analysis including all normal, undamaged glaucoma, and damaged glaucoma specimens. For all models, predictors of the outcomes were considered significant at a $P \leq 0.05$, and generalized estimating equations (GEE) models were used to account for correlations between eyes of the same patient when both eyes were included in the analysis. Sex was not a significant predictor for any of the measured outcomes and was not included in the models. For the outcomes that did not follow a Gaussian distribution, we performed the multivariate analysis on the logarithm of the values. The statistical analyses were performed using the software SAS (version 9.2, SAS Institute Inc., Cary, NC).

Results

Typical Results of Normal and Glaucoma Specimens

Regional Thickness Variation. Normal and glaucoma specimens showed a similar regional variation in thickness for both peripapillary and midposterior sclera. This was characterized by a significantly thicker superior/temporal quadrant than the inferior/nasal quadrant (Fig. 7). In addition, the mean peripapillary scleral thickness was on average 100 μm thicker than the midposterior scleral thickness.

Pressure–Displacement Response. A typical example of the displacement measurements is shown in a normal eye (Fig. 8). A colored contour map of the magnitude of the displacement at $P = 30$ mm Hg for the overall sclera shows that the largest displacements occurred in the nasal–inferior quadrant, where the smallest thickness was measured (Fig. 8a). The maximum displacement magnitude at $P = 30$ mm Hg in the peripapillary region varied from 0.15 to 0.65 mm. The scleral tissues exhibited a nonlinear, rate-dependent, and time-dependent inflation response, showing both hysteresis upon unloading and creep at constant pressure (Figs. 8b, 8c). After the creep test to 15 and 30 mm Hg, the displacements generally recovered after resting for 30 minutes at the reference pressure. For some specimens, the creep deformation was not completely recovered after unloading from 30 mm Hg, suggesting that tissue degradation may have occurred during the creep test to 30 mm Hg. We discarded those specimens and obtained usable data on creep behavior from 20 normal specimens from 15 donors and 13 glaucoma specimens from 10 donors. The displacement response to the two first pressure cycles overlapped. The differences between the two curves were within the error range of the DIC correlation at all pressures, demonstrating the repeatability of the DIC system

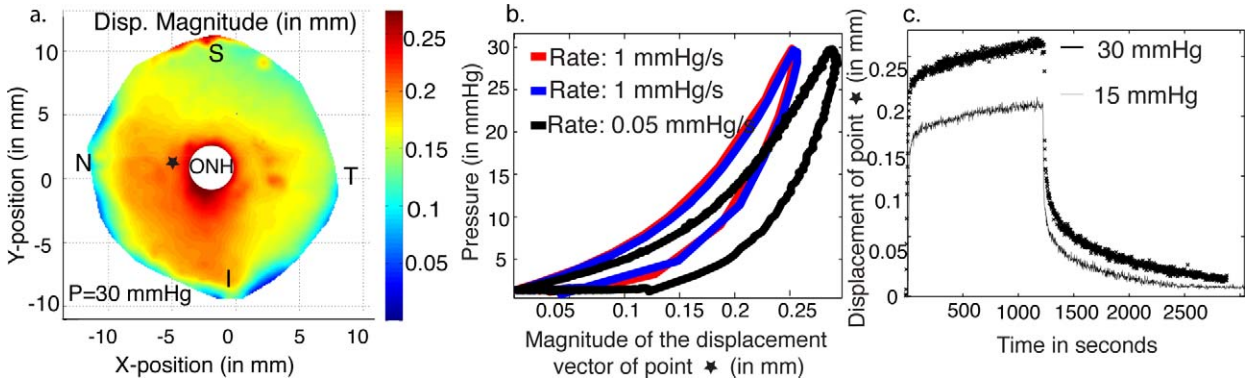

Figure 8. The inflation response of the sclera of a 77-year-old Caucasian male normal donor. (**a**) Colored contour map of the magnitude of the displacement vector ($R = \sqrt{u_x^2 + u_y^2 + u_z^2}$) with red indicating greater displacement. The ONH is not shown. (**b**) The displacement magnitude as a function of pressure for a load–unload test to 30 mm Hg at two different loading rates for the point located in the nasal peripapillary region marked with a star in (a). Note that the two first load–unload tests of the rate dependent test series (rate 1 mm Hg/s, curve red and blue) overlapped, indicating that preconditioning the tissue is not necessary. (**c**) For the same point, the creep tests at 15 and 30 mm Hg showed displacement recovery upon unloading.

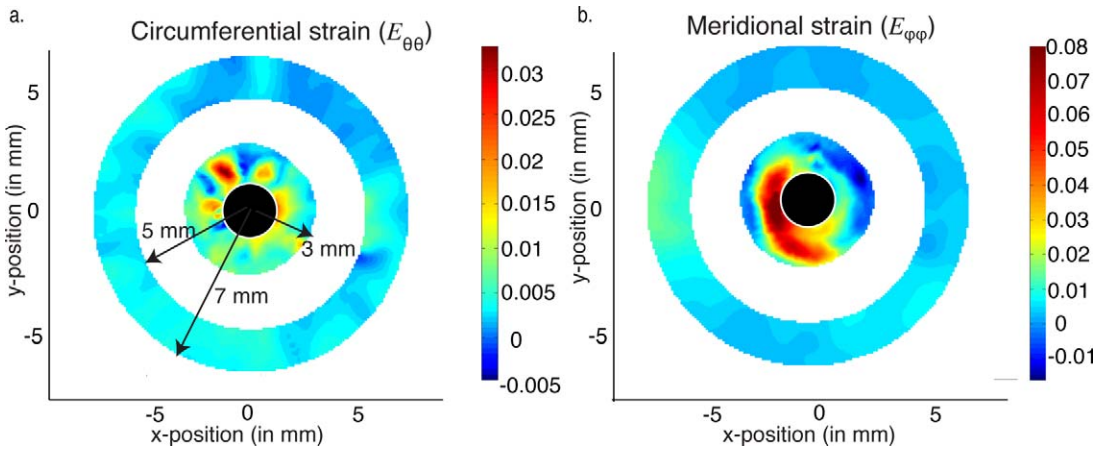

Figure 9. (**a**) Circumferential strain $E_{\theta\theta}$ and (**b**) Meridional strain $E_{\varphi\varphi}$ in both the midposterior and peripapillary sclera for a 77-year-old normal eye.

and also that preconditioning the tissue probably did not affect the results and may not be necessary in future testing (Fig. 8b, red and blue curves).

Strain Response. Figure 9 shows the strain contours in the midposterior and peripapillary sclera for a 77-year-old normal specimen. Almost all specimens experienced larger meridional strains than circumferential strains under inflation in both regions ($P = 0.002$ in the peripapillary sclera and $P = 0.03$ in the midposterior, paired t-test comparing circumferential to meridional strains). Furthermore, for normal specimens, meridional and circumferential strains were larger in the peripapillary sclera than in the midposterior sclera ($P < 0.05$). At 22.5 mm Hg, normal specimens achieved levels of circumferential strains of $E_{\theta\theta} = 1.1\% \pm 1.0\%$ in the peripapillary sclera and $E_{\theta\theta} = 0.37\% \pm 0.4\%$ in the midposterior sclera and greater levels of meridional strains of $E_{\varphi\varphi} = 1.9\% \pm 1.8\%$ and $E_{\varphi\varphi} = 0.47\% \pm 0.36\%$. The spherical approximation of the unloaded midposterior sclera generated an error in strain calculation that was negligible compared to the cross-specimen strain variability (results not shown).

Effects of Age on the Thickness and Stiffness for Normal Specimens

Thickness. For normal specimens, older age was predictive of a thinner sclera ($P = 0.017$, Table 3). When plotted as a linear regression relationship, there was a 15% decrease in thickness between ages 40 and 90 years in normal eyes (Fig. 10, $R^2 = 0.17$).

Stiffness. Both the circumferential and meridional fiber stiffnesses, M_θ and M_φ, in the midposterior sclera were larger in older specimens, though this result was only significant for the circumferential fiber family ($P = 0.0007$, Table 4).

The multivariate regression analysis with age and region as predictors detected that older age was associated with significantly lower strains at 22.5 mm Hg ($P = 0.0006$ for the circumferential strain and $P = 0.011$ for the meridional strain, Table 4). Figure 11a illustrates the stiffening behavior with age observed in normal specimens. The stress–stretch curves were grouped by age showing that younger specimens exhibited larger strains and lower fiber stiffnesses, which corresponded to the initial slope of the loading curves. The circumferential fiber stiffness in the midposterior region is plotted versus age in Figure 11b. The linear regression relationship predicts a threefold increase in stiffness between age 40 and age 80.

No significant age effects were found for the circumferential and meridional strain creep rates at 15 and 30 mm Hg ($P > 0.25$, results not shown).

Table 3. Age Effects on the Average Thickness

Multivariate Regression Results for the Thickness			
Category	**Estimate**	**SE**	***P* Value**
Intercept	1133	24.2	<0.0001
Age	−3.5	1.3	0.017
Region	−112	34	0.0018

Independent Effect of Glaucoma on the Thickness and Inflation Response

Motivated by the results that age influenced the thickness and the eye stiffness, the independent effects of glaucoma were evaluated within two different age groups, 60 to 75 and 76 to 93. In the age group 60 to 75, none of the gradable glaucoma eyes showed axon loss. In this age group, no significant differences were found in the comparison of the thickness,

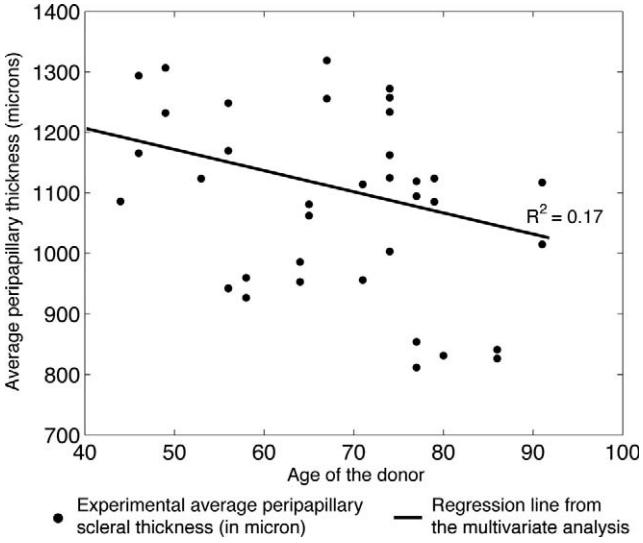

Figure 10. Average peripapillary scleral thickness plotted versus age for normal specimens. The regression line from the model illustrates the age variation of the thickness.

TABLE 4. Age Effects on the Stiffness and Inflation Response

		Multivariate Regression Results for the Inflation Response		
	Category	Estimate	SE	*P* Value
Midposterior material stiffness				
Circumferential fiber stiffness M_θ (MPa)*	Intercept	8.60	0.90	<0.0001
	Age	0.32	0.07	0.0007
Meridional fiber stiffness M_φ (MPa)	Intercept	6.90	1.01	<0.0001
	Age	0.13	0.08	0.14
Midposterior and peripapillary				
log(circumferential strain $E_{\theta\theta}$)†	Intercept	−4.7	0.14	<0.0001
	Age	−0.034	0.0082	0.0006
	Region	−1.15	0.19	<0.0001
log(meridional strain $E_{\varphi\varphi}$)	Intercept	−4.20	0.15	<0.0001
	Age	−0.024	0.009	0.011
	Region	−1.40	0.21	<0.0001

* The circumferential and meridional fiber stiffnesses are calculated from the parameters of the constitutive model.
† The circumferential and meridional strains are calculated at 22.5 mm Hg.

stiffness, and strain creep rates at 15 and 30 mm Hg between normal and glaucoma specimens (Table 5).

In the older age group 76 to 93, regression analyses were performed using the data of 7 damaged glaucoma, 6 undamaged glaucoma, and 12 normal specimens. No ungradable specimens were included. In this age group, damaged glaucoma specimens had a thicker sclera than either normal or undamaged glaucoma specimens ($P = 0.01$ and $P = 0.02$, respectively). When all diagnosed glaucoma specimens were lumped together in one single category, there were no significant differences in thickness compared to normal specimens ($P = 0.09$).

Significant differences in the mechanical response were observed in the peripapillary region between normal and glaucoma specimens. Meridional strains $E_{\varphi\varphi}$ were significantly larger in normal eyes than in both damaged and undamaged glaucoma eyes ($P = 0.007$ and $P = 0.057$). This is illustrated in Figure 12. The ratio of meridional strain to circumferential strain was much larger for the normal group than for both glaucoma groups ($P = 0.004$ and $P = 0.02$). Normal specimens had faster circumferential creep rates at 15 and 30 mm Hg than glaucoma specimens, though the comparison was statistically significant only at 15 mm Hg between normal and undamaged glaucoma specimens ($P = 0.01$). The average values of the peripapillary outcomes are presented in Table 6 and the *P*-values of the ANOVA comparing the different groups in Table 7.

In the midposterior sclera, damaged glaucoma specimens had a faster circumferential creep rate at 15 and 30 mm Hg than normal specimens ($P = 0.026$ and $P = 0.07$) and a faster circumferential creep rate at 15 mm Hg than undamaged glaucoma specimens ($P = 0.04$). However, no differences in creep rates were found in the comparison of normal and undamaged glaucoma specimens.

There were no significant differences between glaucoma and normal specimens in stiffness and strain values in the midposterior sclera. Figure 13 shows the circumferential stress–stretch response of the midposterior region plotted for normal, undamaged glaucoma, and damaged glaucoma specimens, showing a similar response between the three groups.

Effect of Glaucoma Adjusting for the Effects of Age

Both age and glaucoma severity (undamaged or damaged) were added as predictors for scleral properties in a multivariate regression analysis that included all normal, damaged, and undamaged eyes older than 75 (Table 8). The reference diagnosis group was the normal group, and we included only peripapillary outcomes, since glaucoma was not found to be associated with a difference from normal in midposterior scleral parameters. The relationships between glaucoma diagnoses and scleral parameters were in the same direction as those found in the ANOVA analysis (Tables 6, 7). Age was not significantly associated with scleral parameters in this analysis,

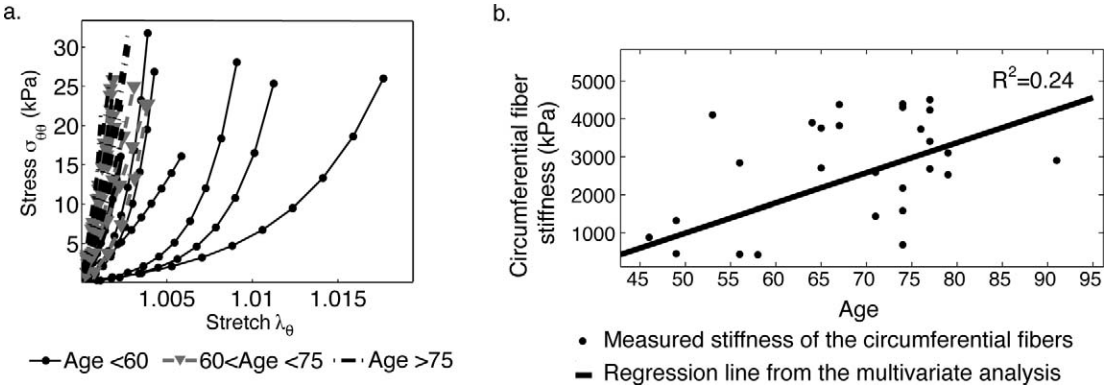

FIGURE 11. (**a**) Circumferential stress versus circumferential stretch for normal specimens. The age effects on the stiffness are clearly seen by separating the eyes into three age groups. (**b**) Stiffness of the circumferential fiber family as a function of age for normal specimens. The regression line from the model predicts a threefold increase in the stiffness between age 40 and 80.

Table 5. Average Peripapillary and Midposterior Sclera Outcomes for the Age Group 60–75 and *P* values for the Comparisons of Normal and Diagnosed Glaucoma Specimens

	Normal Eyes		Diagnosed Glaucoma Eyes		
Number of Eyes/Donors	**14/7**		**7/4**		
Age (avg ± SD)	**69.8 ± 4.3**		**68.8 ± 3.7**		**ANOVA**
Peripapillary	Avg	SD	Avg	SD	*P* values
Thickness (μm)	1157	(129)	1219	(71)	0.3
Circ. strain (%)	0.79	(0.65)	0.69	(0.46)	0.52
Mer. strain (%)	0.94	(0.50)	1.40	(0.94)	0.61
(Mer. strain)/(circ. strain)	1.67	(0.83)	2.19	(1.88)	0.74
Circ. creep at 15 mm Hg	0.26	(0.15)	0.20	(0.09)	0.28
Circ. creep at 30 mm Hg	0.28	(0.18)	0.21	(0.11)	0.14
Midposterior					
Circ. strain (%)	0.22	(0.11)	0.22	(0.07	0.86
Mer. strain (%)	0.38	(0.32)	0.27	(0.12)	0.25
Circ. fiber stiffness (MPa)	13.1	(6.6)	14.3	(4.4)	0.15
Mer. fiber stiffness (MPa)	11.0	(11.5)	12.0	(7.8)	0.35
Stiffening parameter (β)	205	(165)	135	(89)	0.36
(Circ. stiff)/(mer. stiff)*	1.84	(1.0)	1.31	(0.60)	0.25
Circ. creep at 15 mm Hg	0.23	(0.05)	0.19	(0.10)	0.46
Circ. creep at 30 mm Hg	0.25	(0.12)	0.17	(0.06)	0.09

The material anisotropy is defined as the ratio of the circumferential fiber stiffness to meridional fiber stiffness in the midposterior sclera.

* Strains are calculated at 22.5 mm Hg. Circ., circumferential; Mer., meridional; Circ. creep at 15 mm Hg, the strain creep rate in the circumferential direction at 15 mm Hg. The units of the creep rates are: log(%)/log(s).

though the range of age included was less than a 20-year span. To confirm that there was not a significant age effect measurable in our 75 to 93 year group of normals, we repeated the models from Table 4 including only normal specimens of age 75 and older and found no significant associations between age and scleral features ($P > 0.1$, results not shown).

Discussion

This study measured the circumferential and meridional strains in the posterior sclera of normal and glaucomatous human eyes subjected to pressure-controlled inflation. In addition, stresses were calculated in the midposterior sclera and related to strains through an anisotropic model for fibrous tissue. We found that older specimens exhibited a statistically significant stiffer response in both the midposterior and peripapillary regions. Similar stiffening effects with age have been reported in the literature for the cornea[29] and the sclera,[8–10] using various experimental techniques. The effect was typically associated with the accumulation of nonenzymatic glycation-type cross-links of collagen fibrils with age.

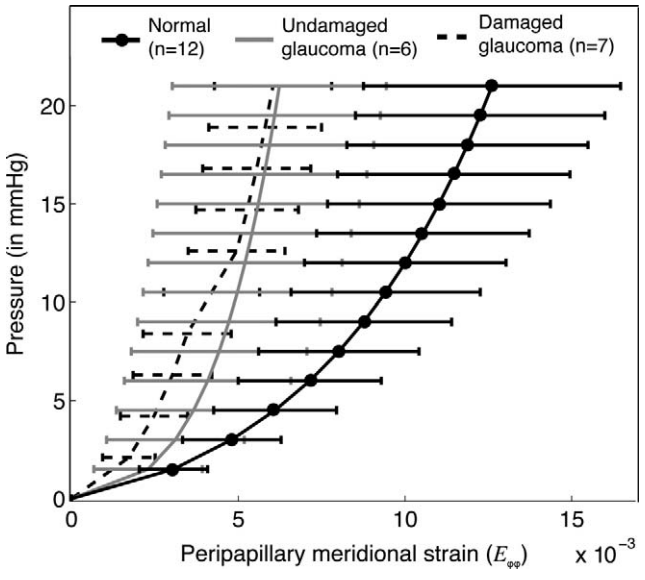

Figure 12. Averaged peripapillary meridional strain versus pressure for normal, undamaged glaucoma, and damaged glaucoma specimens, illustrating the stiffening observed in the meridional direction for diagnosed glaucoma specimens. The length of the error bar represents one standard deviation.

This study detected no significant difference between the stress–strain response of the sclera of normal and glaucoma eyes in the midposterior region. Significant differences were obtained for the strain response in the peripapillary region between normal and glaucoma specimens when the glaucoma tissues were separated by age. Older glaucoma specimens exhibited a smaller strain ratio than normal specimens. In the normal eye, meridional strains were significantly larger than circumferential strains, suggesting a higher density of collagen or elastin fibrils oriented in the circumferential direction, acting as mechanical reinforcements. This observation was consistent with recent histology data[30] (Boote C, et al. *IOVS* 2010;51:ARVO E-abstract 4900) and modeling work.[28] Both approaches showed the existence of a ring of circumferentially oriented fibers around the ONH. In the glaucomatous eye, the meridional strains were significantly lower than in the normal eyes, while no differences were found in circumferential strains. As a result, the meridional direction was as stiff or stiffer than the circumferential direction in glaucomatous specimens. This finding cannot be explained by the observed larger peripapillary thickness among glaucoma specimens as it would similarly affect both directions but is compatible with at least two possible interpretations. One hypothesis is that growth of meridionally oriented fibrillar components occurred in the glaucoma eyes. An alternative hypothesis is that fibrillar components became preferentially cross-linked in the meridional direction with glaucoma. The first interpretation would explain both the larger peripapillary thickness and the lower meridional strains. Whether this phenomenon is a response to

TABLE 6. Average Peripapillary Sclera Outcomes for the Age Group 76 to 93

	All Normals		Undamaged Glaucoma		Damaged Glaucoma	
Number of Eyes/Donors	**12/7**		**6/4**		**7/5**	
Age (Avg ± SD)	**83.1 ± 3.8**		**88.5 ± 2.3**		**83.1 ± 4.1**	
Peripapillary	Avg	SD	Avg	SD	Avg	SD
Thickness (μm)	1001	(142)	989	(114)	1149	(243)
Circ. strain (%)	0.66	(0.31)	0.87	(0.53)	0.74	(0.50)
Mer. strain (%)	1.34	(0.75)	0.58	(0.46)	0.59	(0.61)
(Mer. strain)/(circ. strain)*	2.30	(1.20)	0.70	(0.40)	0.90	(0.70)
Circ. creep at 15 mm Hg	0.27	(0.10)	0.16	(0.11)	0.25	(0.18)
Circ. creep at 30 mm Hg	0.20	(0.15)	0.15	(0.07)	0.16	(0.08)

The ratio of the meridional to circumferential strain is a measure of the anisotropy.

* Strains are calculated at 22.5 mm Hg. Circ. creep at 15 mm Hg is the strain creep rate in the circumferential direction at 15 mm Hg. The units of the creep rates are: log(%)/log(s).

the disease or preceded the development of the disease, and therefore is a risk factor for glaucoma, cannot be distinguished with the present data. This will require biomechanical measurements on the living eye in a longitudinal study. Previous findings in animal experiments that chronic IOP elevation increases scleral stiffness[14] support that this is a response to the disease. Interestingly, glaucoma and normal specimens exhibited identical levels of strains and did not differ in fiber stiffness in the midposterior sclera. This suggests that the effects of glaucoma on the biomechanics of the sclera are concentrated in the tissue immediately surrounding the ONH.

For normal specimens, the creep rates at 15 and 30 mm Hg were not age-dependent. Significant differences in creep rates were found between glaucoma and normal specimens. Undamaged glaucoma specimens had faster circumferential creep rates in the midposterior but slower circumferential creep rates in the peripapillary sclera. The fact that both regions were affected differently could be further evidence of the regionally localized effects of glaucoma. In general, the mechanisms determining creep responses in the sclera are not well understood. These may include the inherent viscoelastic behavior of the proteoglycan matrix and the sliding of collagen fibrils past each other to accommodate the IOP-derived stresses. It is possible that different creep mechanisms are activated at the different stress levels corresponding to $P = 15$ and 30 mm Hg.[31] The response to 15 mm Hg is associated with the knee of the pressure–displacement curve, and deformation may be driven by the uncrimping of collagen fibers. At 30 mm Hg, the loading curve is nearly linear, suggesting that further deformations may arise from stretching of the collagen fibrils. For undamaged glaucoma specimens, slower creep rates in the peripapillary sclera are compatible with the speculated deposition of fibrillar components. This would create a denser network and impede fibril mobility.

For both normal and glaucoma specimens, the peripapillary sclera was approximately 100 μm thicker than the midposterior sclera. In both regions, the thickness distribution was not uniform, with the temporal/superior quadrant consistently thicker than the inferior/nasal quadrant. The average thickness distribution was consistent with the findings of a recent MRI study of spatial variations of scleral thickness.[32] For some specimens, the measured thickness was as large as 1500 μm. To ensure that swelling was not responsible for these large thickness values, we measured the scleral thickness before and after the 4-hour-long test and found negligible differences. For damaged glaucoma specimens, we observed a significantly thicker sclera. The IOP-derived stresses in the sclera scale inversely with the thickness of the scleral wall. Thickening of the sclera in a damaged glaucoma eye might be a protective response to reduce the IOP-derived stresses.

The effect of aging on the scleral thickness of normal specimens has been studied with conflicting outcomes. Watson[33] reported an increase in human scleral thickness with age. Girard[8] reported a significant thinning of the monkey sclera with age. Our findings support a smaller scleral thickness with age in nonglaucoma eyes.

Recent modeling studies[6] have demonstrated the importance of scleral behavior on the biomechanics of the ONH. Pressure-induced stresses in the peripapillary sclera are magnified at the LC, and the strains transmitted to the RGC axons are determined by the material properties of the peripapillary sclera and LC. Finite element analyses of the posterior sclera have been used extensively to evaluate the effect of scleral properties on the stress and strain state of the LC.[6,28] The predictive ability of computational models relies on the accuracy of the material description. Uniaxial and biaxial strip tests (e.g., Eilaghi et al.[18]) provide a direct measurement of the stress–strain behavior of the tissue but are commonly associated with large preconditioning effects, which suggests significant alterations to the fibrous microstructure of the tissue. Inflation test methods apply a biaxial loading state that is closer to the physiological loading conditions of the eye without the significant effects of preconditioning. We believe that material parameters obtained from inflation tests represent a more accurate description of the mechanical behavior of the sclera. A disadvantage of inflation methods is that stresses cannot be measured directly. We calculated the circumferential and meridional stresses from the pressure and deformed geometry by modeling the scleral cup as a thin ellipsoidal

TABLE 7. *P* Values From the ANOVA Comparing the Average Peripapillary Outcomes in the Age Group 76 to 93

	Normals vs. Undamaged Glaucoma	Normals vs. Damaged Glaucoma	Damaged vs. Undamaged Glaucoma
Thickness	0.97	0.01	0.02
Circ. strain (%)	0.45	0.90	0.71
Mer. strain (%)	0.007	0.057	0.67
(Mer. strain)/(circ. strain)*	0.004	0.02	0.25
Circ. creep at 15 mm Hg	0.014	0.70	0.13
Circ. creep at 30 mm Hg	0.38	0.62	0.86

Circ. creep at 15 mm Hg is the circumferential strain creep rate at 15 mm Hg. The units of the creep rates are: log(%)/log(s).

* The ratio of the meridional to circumferential strain is a measure of the anisotropy.

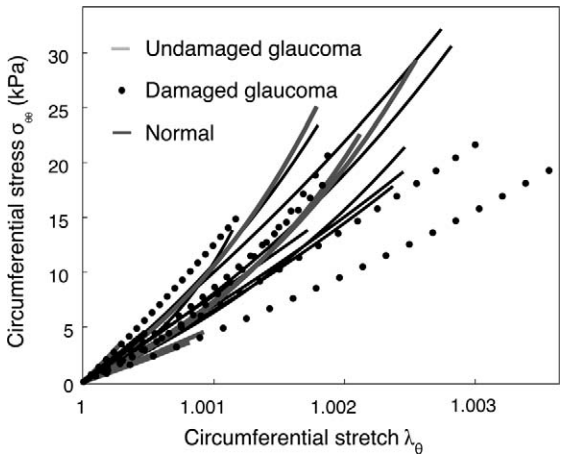

Figure 13. Circumferential stress versus circumferential stretch in the midposterior sclera for normal, damaged, and undamaged glaucoma specimens older than 75. There were no statistically significant differences in stiffness or level of strain at 22.5 mm Hg between glaucoma and normal specimens.

membrane (equation 3). We are currently validating this assumption by applying finite element models to simulate the inflation tests and optimization methods to calculate the material parameters.[34] The models incorporate a detailed description of the collagen structure obtained from wide-angle X-ray scattering (WAXS) measurements of the collagen structure of a subset of inflation tested normal and glaucoma specimens (Boote C, et al. *IOVS* 2010;51:ARVO E-abstract 4900).

Several limitations should be considered when interpreting the results of this study. First, the DIC displacements were computed with an inherent uncertainty that was experimentally measured to be 8 μm. Numerical differentiation of the displacements should add to the uncertainty in the strain calculation. To prevent excessively noisy strain contours, we smoothed the displacements. This technique did not affect the average value of the strains but removed unrealistic values. In this paper, we used the regionally averaged strains over the entire peripapillary and midposterior regions for statistical comparison. In the midposterior sclera, strains were relatively uniform and small. It is possible that some local values of strains were within the uncertainty of the DIC measurements. This may explain why no significant differences in the mechanical response of normal and glaucoma specimens were detected in this region. However, the average strain values were consistent with recent experimental work on the monkey eye[8] and on the human eye.[18] Peripapillary scleral strains were larger, and measurement uncertainty was not an issue in this region. Our laboratory is currently implementing the recommendations of Ke et al.[25] to increase the resolution in out-of-plane displacement calculation. With a better resolution, smaller differences associated with glaucoma that were not detectable with the current configuration might be found. In both regions, comparing the average biomechanical measures did not examine the regional variations in material properties, thickness, and curvatures. In the peripapillary sclera, some specimens exhibited long-range strain gradients. By taking the average over the entire region, we ignored these local variations that may be important in the deformation state of the LC and the development of glaucoma. The midposterior sclera exhibited a more uniform strain response and thickness profile, suggesting that the material properties were more homogeneous in this region. In our current finite element modeling studies, regional variations of the material behavior are introduced from the spatial variations of the collagen fiber structure. The preliminary WAXS data (Boote C, et al. *IOVS* 2010;51:ARVO E-abstract 4900) does not show abrupt changes in the midposterior fiber structure away from the peripapillary region. It is likely that the variations of material behavior within the midposterior sclera are small compared to those in the peripapillary sclera.

Second, in modeling the stress–strain response of the midposterior sclera, we assumed that the fibrillar components were oriented only in the circumferential and meridional directions. Recent histologic studies have shown that the fibers are instead dispersed around one preferred direction.[8,30] When we included the dispersion of fibers in the model for the posterior sclera, we could not find a unique solution to the optimization problem because of the larger number of parameters. This model was not used in this study as the comparison between normal and glaucoma specimens relies on the strict convexity of the optimization problem. The thin membrane model for stress calculation in the midposterior sclera, which neglected the effects of transverse shear stresses, bending stresses, and through-thickness variations in the membrane stresses, are not valid in the peripapillary sclera.Therefore, we used strains to compare the mechanical response of the specimens. Strains are dependent on the geometry and boundary conditions and do not measure the material response. However, they provide valuable information in studying the biomechanics of glaucoma. Strains in the peripapillary sclera are transmitted to the LC. Understanding the boundary conditions of the LC can help to construct more realistic models that investigate local measures of the ONH stress–strain behavior.

Third, there are inherent difficulties in confirming the glaucoma status of donor eyes obtained from eye banks and commercial entities such as NDRI. Many studies simply accept the statement from a providing agency or eye bank that the patient had glaucoma. It is rare to obtain actual medical records documenting glaucoma diagnosis and treatment because of privacy regulations and practical considerations. We evaluated the optic nerve cross-section of all diagnosed glaucoma eyes and were able to assess the severity of axonal damage in 18 out of 22 glaucoma specimens. The ungradable nerves had postmortem autolysis. By differentiating between

Table 8. Multiple Regression Models with Normal Specimens as the Reference Group Including All Normal and Glaucoma Specimens Older than 75

	log(Circ. Strain)		log(Mer. Strain)		(Circ. Strain)/(Mer. Strain)	
	Estimate	***P* Value**	**Estimate**	***P* Value**	**Estimate**	***P* Value**
Intercept	−5.14	<0.0001	−4.4	<0.0001	0.71	0.01
Age	−0.02	0.55	−0.007	0.87	0.01	0.78
Undamaged	0.30	0.46	−1.57	0.007	−1.84	0.007
Damaged	−0.06	0.85	−0.97	0.05	−0.77	0.16

undamaged and damaged nerves, we found differences between groups. Investigators are encouraged to perform optic nerve damage assessment to validate the state of glaucoma in the tissues that they utilize. In multivariate analysis, we found a significant age–diagnosis interaction in some parameters. This indicates that, in addition to the normal aging effect, there is a significant additional relationship between age and glaucoma in the features that we studied. This is expected, considering that the incidence of glaucoma increases with age and that older glaucoma patients are more likely to have had the disease for a longer period than younger ones. Broman et al.[35] estimated that the average European-derived person with OAG at age 50 has had the disease for 7 years, while a 90-year-old with OAG has had it for an average duration of 13 years. Whatever the effects of glaucoma on the scleral inflation behavior, they would have had nearly twice as long to influence the results in the oldest donors compared to the younger ones. The strength of human tissue studies over monkey or other animal models is that of studying the spontaneous human disease. One weakness, as indicated here, is that we have insufficient data on disease exposure.

A fourth weakness is that any in vitro inflation protocol does not replicate in vivo conditions. Postmortem swelling of the sclera may occur before testing and affect the mechanical behavior of the tissue. The specimens were tested at room temperature. Testing at body temperature, without in vivo mechanisms to maintain collagen integrity, would have accelerated tissue degradation. The creep behavior is affected by the temperature, and we would expect to observe faster creep rates at 37°C.[20] Our objective was to compare the mechanical behavior of normal and diseased tissue. Differences that were found at room temperature are likely to exist at body temperature. Gluing the sclera also introduces stress concentrations near the holder that are not physiological. In our experiments, there were positive circumferential and meridional creep rates at 15 mm Hg, a physiological IOP. Phillips[36] showed that the in vivo creep behavior of tree shrew eyes was different. While the pressure of the eye was kept at 100 mm Hg, the axial length decreased with time. This was speculated to occur through the action of contractile myofibroblasts. None of the postmortem human specimens that we tested exhibited such a behavior. We cannot tell whether there are no such contractile elements in the human sclera or whether they do not survive patient death.

In summary, the thickness and biomechanical response of human glaucoma eyes differed from normal eyes. Glaucoma eyes were thicker, and they exhibited a stiffer meridional strain response, a smaller ratio of meridional to circumferential strains, and slower circumferential creep rates in the peripapillary sclera. These data suggest either that scleral responses are inherently related to development of glaucoma damage or that the process that leads to glaucoma damage alters scleral response, or both.

References

1. Morrison JC, Johnson EC, Cepurna W, Jia L. Understanding mechanisms of pressure-induced optic nerve damage. *Prog Retin Eye Res*. 2005;24:217–240.
2. Hernandez MR, Pena JDO. The optic nerve head in glaucomatous optic neuropathy. *Arch Ophthalmol*. 1997;115:389–395.
3. Quigley HA. Neuronal death in glaucoma. *Prog in Ret and Eye Res*. 1997;18:39–57.
4. Ethier CR. Scleral biomechanics and glaucoma—a connection? *Can J Ophthalmol*. 2006;41:9–12, 14.
5. Burgoyne CF, Downs JC, Bellezza AJ, Suh JKF, Hart RT. The optic nerve head as a biomechanical structure: a new paradigm for understanding the role of IOP-related stress and strain in the pathophysiology of glaucomatous optic nerve head damage. *Prog Retin Eye Res*. 2005;24:39–73.
6. Sigal IA. Interaction between geometry and mechanical properties on the optic nerve head. *Invest Ophthalmol Vis Sci*. 2009;50:2785–2795.
7. Sigal IA, Flanagan JG, Ethier CR. Factors influencing optic nerve head biomechanics. *Invest Ophthalmol Vis Sci*. 2005; 11:4189–4199.
8. Girard MJA, Suh JKF, Bottlang M, Burgoyne CF, Downs JC. Scleral biomechanics in the aging monkey eye. *Invest Ophthalmol Vis Sci*. 2009;50:5226–5237.
9. Myers KM, Cone FE, Quigley HA, Gelman S, Pease ME, Nguyen TD. The in vitro inflation response of the mouse sclera. *Exp Eye Res*. 2009;91:866–875.
10. Schultz DS, Lotz JC, Lee SM, Trinidad ML, Stewart JM. Structural factors that mediate scleral stiffness. *Invest Ophthalmol Vis Sci*. 2008;49:4232–4236.
11. Quigley HA, Brown A, Dorman-Pease MA. Alterations in elastin of the optic nerve head in human and experimental glaucoma. *Br J Ophthalmol*. 1991;75:552–557.
12. Downs JC, Suh JKF, Thomas KA, Bellezza AJ, Hart RT, Burgoyne CF. Viscoelastic material properties of the peripapillary sclera in normal and early-glaucoma monkey eyes. *Invest Ophthalmol Vis Sci*. 2005;46:540–546.
13. Hommer A, Fuchsjäger-Maryl G, Resch H, Vass C, Garhofer G, Schmetterer L. Estimation of the ocular rigidity based on measurement of pulse amplitude using pneumotonometry and fundus pulse using laser interferometry in glaucoma. *Invest Ophthalmol Vis Sci*. 2008;49:4046–4050.
14. Girard MJA, Suh JKF, Bottlang M, Burgoyne CF, Downs JC. Biomechanical changes in the sclera of monkey eyes exposed to chronic IOP elevations. Invest Ophthalmol Vis Sci. 2011;52: 5656–5669.
15. Cone FE, Gelman SE, Son JL, Pease ME, Quigley HA. Differential susceptibility to experimental glaucoma among 3 mouse strains using bead and viscoelastic injection. *Exp Eye Res*. 2010;91:415–424.
16. Phillips JR, Khalaj M, McBrien NA. Induced myopia associated with increased scleral creep in chick and tree shrew eyes. *Invest Ophthalmol Vis Sci*. 2000;41:2028–2034.
17. Boland MV, Quigley HA. Risk factors and open-angle glaucoma: concepts and applications. *J Glaucoma*. 2007;16:406–418.
18. Eilaghi A, Flanagan JG, Simmons CA, Ethier CR. Effects of scleral stiffness properties on optic nerve head biomechanics. *Annals of Biomed Eng*. 2009;38:1586–1592.
19. Girard MJA, Suh JFK, Hart RT, Burgoyne CF, Downs JC. Effects of storage time on the mechanical properties of rabbit peripapillary sclera after enucleation. *Curr Eye Res*. 2007;32: 465–470.
20. Greene PR, McMahon TA. Scleral creep versus temperature and pressure in vitro. *Exp Eye Res*. 2000;29:527–537.
21. Kendell KR, Quigley HA, Kerrigan LA, Pease ME, Quigley EN. Primary open-angle glaucoma is not associated with photoreceptor loss. *Invest Ophthalmol Vis Sci*. 1995;36:200–205.
22. Boyce BL, Grazier JM, Jones RE, Nguyen TD. Full-field deformation of bovine cornea under constrained inflation conditions. *Biomaterials*. 2008;29:3896–3904.
23. Myers KM, Coudrillier B, Boyce BL, Nguyen TD. The inflation response of bovine sclera. *Acta Biomater*. 2010;6:4327–4335.
24. Ye SG, Harasiewicz KA, Pavlin CJ, Foster FS. Ultrasound characterization of ocular tissue in the frequency range from 50MHz to 100MHz. *IEEE Trans Ultrason Ferroelec Freq Control*. 2010;42:8–14.
25. Ke XD, Schreier HW, Sutton MA, Wang YQ. Error assessment in stereo-based deformation measurements, II: experimental

validation of uncertainty and bias estimates. Exp Mech. 2011; 51:423–441.

26. Anderson K, El-Sheikh A, Newson T. Application of structural analysis to the mechanical behaviour of the cornea. *J. R. Soc. Interface*. 2004;1:3–15.
27. Flügge W. *Stresses in Shells*. 1st ed. Berlin, Göttingen, Heidelberg: Springer-Verlag; 1960.
28. Grytz R, Mesch G. The collagen fibril architecture in the lamina cribrosa and peripapillary sclera predicted by a computational remodeling approach. *Biomech Model Mechanobiol*. 2010;10:371–382.
29. Elsheikh A, Wang D, Brown M, Rama P, Campanelli M, Pye D. Assessment of corneal biomechanical properties and their variation with age. *Curr Eye Res*. 2007;32:11–19.
30. Yan D, McPheeters S, Johnson G, Utzinger U, Vande Geest JP. Microstructural differences in the human posterior sclera as a function of age and race. *Invest Ophthalmol Vis Sci*. 2011;52: 821–829.
31. Nguyen TD, Jones RE, Boyce BL. A nonlinear anisotropic viscoelastic model for the tensile behavior of the corneal stroma. *J Biomech Eng*. 2008;130:041020.
32. Norman RE, Flanagan JG, Rausch SMK, et al. Dimensions of the human sclera: thickness measurement and regional changes with axial length. *Exp Eye Res*. 2010;90:277–284.
33. Watson PG, Young RD. Scleral structure, organization and disease. A review. *Exp Eye Res*. 2004;78:609–623.
34. Nguyen TD, Boyce BL. An inverse finite element method for determining the anisotropic properties of the cornea. *Biomech Model Mechanobiol*. 2011;10:323–337.
35. Broman AT, Quigley HA, West SK, et al. Estimating the rate of progressive visual field damage among those with open-angle glaucoma from cross-sectional data. *Invest Ophthalmol Vis Sci*. 2008;49:66–76.
36. Phillips JR, McBrien NA. Pressure-induced changes in axial eye length of chick and tree shrew: significance of myofibroblasts in the sclera. *Invest Ophthalmol Vis Sci*. 2009;45:758–763.
37. Holzapfel GA. *Nonlinear Solid Mechanics: a Continuum Approach for Engineering*. Chichester, UK: Wiley; 2000.

Appendix A: Constitutive Relation

We assumed the existence of two unidirectional families of fibers, with direction $\mathbf{e}_\theta$ (fibers oriented circumferentially) and $\mathbf{e}_\varphi$ (fibers oriented along the meridian). The midposterior sclera was characterized by a strain energy W, sum of the contribution of an isotropic, incompressible matrix and the contribution of the reinforcing collagen fibers:[37]

$$W = W_{\text{matrix}}\Big(I_1(\mathbf{C}),J\Big) + W_{\text{fiber}}\Big(I_4(\mathbf{C})\Big) + W_{\text{fiber}}\Big(I_6(\mathbf{C})\Big) \quad (8)$$

where $\mathbf{C} = \mathbf{F^T F}$ is the right Cauchy-Green deformation tensor, $\mathbf{F}$ is the deformation gradient, $I_1(\mathbf{C})$ and $I_3(\mathbf{C}) = J^2$ are the first and third invariants of $\mathbf{C}$. $I_4(\mathbf{C}) = \lambda_\varphi^2$ and $I_6(\mathbf{C}) = \lambda_\theta^2$ are the pseudo-invariants of $\mathbf{C}$ that characterized the fiber family with direction $\mathbf{e}_\varphi$ and $\mathbf{e}_\theta$ and described the inherent anisotropy of the tissue due to the collagen alignment. The matrix was modeled as an incompressible Neo-Hookean model with shear modulus μ,

$$W_{\text{matrix}}(I_1,J) = \frac{\mu}{2}(I_1 - 3) + p(J - 1). \quad (9)$$

For the fiber strain energy density, we used an exponential model to capture the stiffening behavior at elevated pressure,

$$W_{\text{fiber}}(\lambda) = \frac{\alpha}{\beta}\Big[\exp\Big(\beta(\lambda^2 - 1)\Big) - \beta\lambda^2\Big]. \quad (10)$$

β is the strain stiffening parameter and $4\alpha\beta$ denotes the stiffness of the fiber family. The Cauchy stress tensor $\boldsymbol{\sigma}$ is derived from the strain energy density W using the theory of hyperelasticity $\boldsymbol{\sigma} = 2J^{-1}\mathbf{F}\left(\frac{\partial C}{\partial W}\right)\mathbf{F}^T$. The biaxial boundary condition ($\sigma_{rr} = 0$) was used to determine the value of the pressure p:

$$\begin{aligned}\boldsymbol{\sigma}_{\theta\theta} &= \mu\left(\lambda_\theta^2 - \frac{1}{\lambda_\theta^2\lambda_\varphi^2}\right) + 2\alpha_\theta\lambda_\theta^2\Big[\exp\Big(\beta(\lambda_\theta^2 - 1)\Big) - 1\Big],\\ \boldsymbol{\sigma}_{\varphi\varphi} &= \mu\left(\lambda_\varphi^2 - \frac{1}{\lambda_\theta^2\lambda_\varphi^2}\right) + 2\alpha_\varphi\lambda_\varphi^2\Big[\exp\Big(\beta(\lambda_\varphi^2 - 1)\Big) - 1\Big].\end{aligned} \quad (11)$$

Appendix B: In-Plane Shear Strains in the Midposterior Sclera

The in-plane shear strain, defined as $E_{\theta\varphi} = \frac{1}{2}\mathbf{t}_\theta \cdot \mathbf{t}_\varphi$, describes the relative distortion of the initially orthogonal meridional and circumferential directions. The average value of $E_{\theta\varphi}$ over the entire midposterior sclera was compared to the averaged circumferential and meridional strains for all specimens (Table A1). On average, the ratio of the averaged in-plane shear strain over the averaged normal strains was 0.068 ± 0.055 for normal specimens and 0.078 ± 0.053 for diagnosed glaucoma specimens. This strain ratio was not significantly different between normal and diagnosed glaucoma specimens ($P = 0.61$).

Table A1. Comparison of the Averaged Midposterior In-Plane Shear Strain and the Averaged Midposterior Normal Strains for Normal (left) and Diagnosed Glaucoma (right) Specimens

Normal Specimens					Glaucoma Specimens				
	Averaged Normal Strains (%)		Averaged Shear Strain (%)	Shear to Normal Strain Ratio		Averaged Normal Strains (%)		Averaged Shear Strain (%)	Shear to Normal Strain Ratio
ID	$E_{\varphi\varphi}$	$E_{\theta\theta}$	$E_{\theta\varphi}$	$2E_{\theta\varphi}/(E_{\varphi\varphi}+E_{\theta\theta})$	ID	$E_{\varphi\varphi}$	$E_{\theta\theta}$	$E_{\theta\varphi}$	$2E_{\theta\varphi}/(E_{\varphi\varphi}+E_{\theta\theta})$
4	0.753	0.885	0.002	0.002		Undamaged Glaucoma Specimens			
5	0.366	0.472	−0.027	0.064	1	0.306	0.226	0.022	0.084
6	0.486	0.367	−0.016	0.037	2	0.267	0.340	−0.029	0.096
7	0.158	0.194	−0.025	0.142	3	0.196	0.181	−0.013	0.068
8	0.185	0.389	−0.004	0.015	15	0.211	0.186	0.006	0.028
9	0.242	0.152	0.045	0.226	16	0.048	0.244	−0.027	0.183
10	0.397	0.162	−0.020	0.072	17	0.445	0.255	−0.022	0.064
11	0.217	0.184	−0.024	0.122	18	0.304	0.204	−0.021	0.083
12	0.496	0.205	−0.035	0.101	19	1.743	1.095	−0.106	0.074
13	0.279	0.326	−0.003	0.008	27	0.220	0.273	0.017	0.071
14	0.185	0.144	−0.003	0.016	28	0.243	0.151	0.004	0.021
22	0.462	0.428	−0.007	0.015	45	0.318	0.891	0.027	0.044
29	0.583	1.253	−0.135	0.147	47	0.146	0.222	−0.009	0.047
30	0.384	0.294	0.033	0.098	49	0.236	0.260	−0.034	0.136
31	0.442	0.279	−0.015	0.040	50	0.317	0.488	−0.013	0.033
32	1.186	0.472	−0.052	0.063					
33	0.386	0.239	0.004	0.013		Damaged Glaucoma Specimens			
34	0.205	0.190	0.028	0.142	20	0.146	0.112	−0.002	0.018
35	0.076	0.128	−0.007	0.066	21	0.196	0.268	−0.005	0.023
36	0.139	0.140	−0.008	0.058	24	0.126	0.159	−0.001	0.009
37	0.350	0.219	0.007	0.025	25	0.182	0.189	0.029	0.154
38	0.192	0.145	−0.007	0.041	26	0.209	0.184	0.017	0.086
39	0.825	0.986	−0.089	0.099	44	0.419	1.349	0.011	0.012
40	1.400	1.368	0.069	0.050	46	0.191	0.392	0.016	0.054
41	0.286	0.400	−0.027	0.077					
42	0.193	0.235	−0.002	0.007					
43	0.289	0.772	−0.027	0.050					
48	0.150	0.137	−0.031	0.213					
51	0.192	0.290	0.010	0.044					
52	0.167	0.217	−0.008	0.043					
53	0.142	0.106	0.010	0.082					
54	0.179	0.196	0.010	0.053					
55	0.273	0.539	0.010	0.025					
56	0.179	0.196	0.010	0.053					

On average over all specimens, the ratio of averaged in-plane shear to normal strain was 0.067 ± 0.052.